

# Excitation functions of related temperatures of $\eta$ and $\eta^0$ emission sources from squared momentum transfer spectra in high-energy collisions

Qi Wang<sup>1,\*</sup>, Fu-Hu Liu<sup>2,†</sup>, Khusniddin K. Olimov<sup>3,4‡</sup>

<sup>1</sup>*College of Basic Courses, Shanxi Institute of Energy, Jinzhong 030600, China*

<sup>2</sup>*Institute of Theoretical Physics, State Key Laboratory of Quantum Optics and Quantum Optics Devices  
& Collaborative Innovation Center of Extreme Optics, Shanxi University, Taiyuan 030006, China*

<sup>3</sup>*Physical-Technical Institute of Uzbekistan Academy of Sciences,  
Chingiz Aytmatov str. 2b, Tashkent 100084, Uzbekistan*

<sup>4</sup>*National University of Science and Technology MISIS (NUST MISIS), Almalyk Branch, Almalyk, Uzbekistan*

**Abstract:** The squared momentum transfer spectra of  $\eta$  and  $\eta^0$ , produced in high-energy photon-proton ( $\gamma p \rightarrow \eta(\eta^0) + p$ ) processes in electron-proton ( $ep$ ) collisions performed at CEBAF, NINA, CEA, SLAC, DESY, and WLS are analyzed. The Monte Carlo calculations are used in the analysis of the squared momentum transfer spectra, where the transfer undergoes from the incident  $\gamma$  to emitted  $\eta(\eta^0)$  or equivalently from the target proton to emitted proton. In the calculations, the Erlang distribution and Tsallis-Levy function are used to describe the transverse momentum ( $p_T$ ) spectra of emitted particles. Our results show that the average transverse momentum ( $\langle p_T \rangle$ ), the initial-state temperature ( $T_i$ ), and the final-state temperature ( $T_0$ ) roughly decrease from the lower center-of-mass energy ( $W$ ) to the higher one in the concerned energy range of a few GeV, which is different from the excitation function from heavy-ion collisions in the similar energy range.

**Keywords:** Initial-state temperature; final-state temperature; squared momentum transfer; Erlang distribution; Tsallis-Levy function

PACS numbers: 12.40.Ee, 14.40.-n, 24.10.Pa, 25.75.Ag

## I. INTRODUCTION

Abundant experimental data produced at the Large Hadron Collider (LHC) and Relativistic Heavy Ion Collider (RHIC) are helpful for scientists to study production of Quark-Gluon Plasma (QGP) and the evolution of the collision system. In the process of high-energy heavy-ion collisions, the time evolution of the collision system roughly consists of five stages which are: flight of incoming nuclei, beginning of collisions, strongly-coupled QGP (sQGP), mixed phase, and hadron gas, respectively [1]. In each stage, the evolution picture and property of the collision system, and the distribution law and property of the produced particles, are possibly different from others, because some particles are produced in the earlier processes and others are produced in the last stage.

In the initial stages, two nuclei with the shape of pancake due to the Lorentz contraction move toward each other and collide violently. Because of the transformation from the kinetic energy of the particles to the huge amount of the

---

\* wangqi@sxie.edu.cn; 18303476022@163.com

† Correspondence: fuhuliu@163.com; fuhuliu@sxu.edu.cn

‡ Correspondence: khkolimov@gmail.com; kh.olimov@uzsci.net

thermal energy of the system, after a short period of time ( $\sim 1 \text{ fm}/c$ ), QGP is produced which is the extremely hot and dense matter [2–5]. In the stages of mixed phase and hadron gas, due to the inflation and cooling down of the system, the hadron matter evolves until only color-neutral states are created. In high-energy collisions, the excitation and equilibrium degrees of the system are considered as the important characteristics which can help us to study the mechanism of the nuclear reaction and the characteristics of the system evolution [6–15].

In the whole process of high-energy collisions, one can use different temperatures to describe the excitation degree of the system or emission source at different stages [16–23]. At the first place, one can choose the initial-state temperature ( $T_i$ ) to describe the excitation degree of the system at the beginning of collisions. At the second place, one can use the critical temperature ( $T_c$ ) and the chemical freeze-out temperature ( $T_{ch}$ ) to describe the excitation degree of the system in which the hadron matter appears and chemical freeze-out happens separately. At the last place, one can use the kinetic freeze-out or final-state temperature ( $T_{kin}$  or  $T_0$ ) and the effective temperature ( $T_{eff}$ ) to describe the excitation degree of the system at the kinetic freeze-out. Here,  $T_{eff}$  includes in addition the flow effect and can be compared with  $T_{kin}$  or  $T_0$ .

As a useful tool for describing the excitation degree of the system,  $T_i$  represents the temperature of the system or emission source at the initial-stage of collisions [24, 25]. This initial-stage refers to a very short stage after the thermalization at the beginning of collisions. To obtain  $T_i$ , we have several methods. The first method is to solve the state equation of QGP with fluid model [19]. The second one is to solve the equation for isentropic expansion in relativistic fluid mechanics [16]. The last one is to use the transverse momentum ( $p_T$ ) spectra directly, or use various distributions or functions to fit the  $p_T$  spectra. The last method has special advantages of accuracy and efficiency. This is because there is no need to study the concrete evolution process from QGP or sQGP to hadron phase, but analyze the  $p_T$  spectra themselves. Usually, we can use the Erlang distribution [26–28], Hagedorn function [29], and Tsallis-Levy function [30] for fitting the  $p_T$  spectra to obtain  $T_i$ , but in this paper, only the Erlang distribution is selected due to it being the origin of multiple sources in the multi-source thermal model [26–28].

The final-state temperature  $T_0$  known as the kinetic freeze-out temperature represents the temperature of the system or emission source at the kinetic freeze-out stage. At this stage, the interactions between various particles are negligible, and there is no further elastic collisions in the system.  $T_0$  can be extracted by using the certain distribution or function in fitting the  $p_T$  spectra, and used to describe the excitation degree of the system.  $T_{eff}$  is similar to  $T_0$ , but there is no influence of flow effect in  $T_0$ . In our previous work [24, 25], we have used the Tsallis-Levy function [30] in fitting the  $p_T$  spectra to estimate  $T$  as  $T_{eff}$ . In some small systems such as  $\gamma p$  and  $\gamma^* p$  collisions, we have  $T_0 \approx T$ , because the flow effect are negligible. In the  $\gamma p$  collisions discussed in this work, we use the Tsallis-Levy function [30] in fitting the  $p_T$  spectra to extract  $T$  ( $T_{eff}$ ) as  $T_0$  and study the characteristics of the system at the last stage. As for the other temperature types, we do not discuss them in our work anymore.

One can use some parameters to describe the equilibrium degree of the system. By fitting the  $p_T$  spectra with the Tsallis distribution [31, 32], the entropy index  $q$  is extracted. Generally, if  $q$  is closer to 1, the system is closer to equilibrium, or the equilibrium degree of the system is higher. In the absence of the Tsallis distribution [31, 32], one can use the Hagedorn function [29] or Tsallis-Levy function [30] alternatively. In the fitting process,  $q$  can be abstracted by introducing  $n$ , which is used to describe the equilibrium degree of the system indirectly due to  $n = 1/(q - 1)$ . In this work, let  $n$  be fixed, then we may obtain  $T_i$  and  $T_0$  more conveniently to describe the excitation degree of the system. It should be noted that when considering the equilibrium issue, small systems are also possible because we consider a large number of events within the framework of giant canonical ensemble.

To obtain the above-mentioned temperatures and  $\langle p_T \rangle$ , we need to use the  $p_T$  spectra. In the absence of the  $p_T$  spectra, we can use the squared momentum transfer ( $|t|$ ) spectra alternatively. The squared momentum transfer is one of the Mandelstam variables which consists of the four-momentum of the concerned particles [33]. In the fitting process, the squared momentum transfer spectra can not be fitted by those distributions and functions directly. Instead, we can obtain many concrete  $p_T$  satisfying certain distribution, then we can obtain many concrete values of the squared momentum transfer with the Monte Carlo calculation. Finally, we can obtain the distribution of the

squared momentum transfer.

In this paper, the squared momentum transfer spectra of  $\eta$  and  $\eta^0$ , produced in high-energy  $\gamma p$  collisions performed at the Continuous Electron Beam Accelerator Facility (CEBAF) [34], the Daresbury Laboratory electron synchrotron NINA [35], the Cambridge Electron Accelerator (CEA) [36], the Stanford Linear Accelerator Center (SLAC) [37], the Deutsches Elektronen-Synchrotron (DESY) [38], and the Wilson Laboratory Synchrotron (WLS) [39] are fitted by the results obtained with the Monte Carlo method. These experimental data are measured at different center-of-mass energies ( $W$ ) and incident photon energies ( $E_\gamma$ ).

The remainder of this article is structured as follows. The formalism and method are described in Section 2. Results and discussion are given in Section 3. In section 4, we give our summary and conclusions.

## II. PICTURE AND FORMALISM

### i) *The Erlang distribution*

The Erlang distribution which describes the  $p_T$  spectra and multiplicity distribution can be obtained from the multi-source thermal model [26–28], where the multiplicity is defined as the number of particles produced in an event. The model assumes that multiple sources are formed and contribute to  $p_T$  of considered particles in collision process. These sources are considered as nucleons or partons if we study the formation of nucleon clusters (nuclear fragments) or particles. Generally speaking, it is enough to use one or two-component Erlang distribution in fitting the  $p_T$  spectra.

The Erlang distribution is the convolution of multiple exponential distributions [26–28]. Every exponential distribution represents the transverse momentum ( $p_t$ ) distribution obeyed by a parton, and can be regarded as

$$f(p_{tj}) = \frac{1}{\langle p_t \rangle} \exp\left(-\frac{p_{tj}}{\langle p_t \rangle}\right). \quad (1)$$

Here,  $j$ ,  $p_{tj}$ , and  $\langle p_t \rangle$  refer to the index of participant partons, the transverse momentum which depends on  $j$ , and the average contribution of participant partons to  $\langle p_T \rangle$  of the considered particles, respectively.

It is assumed that  $n_s$  partons contribute to  $p_T$  of a given particle. We have the Erlang  $p_T$  distribution to be

$$f_1(p_T) = \frac{1}{N} \frac{dN}{dp_T} = \frac{p_T^{n_s-1}}{(n_s-1)! \langle p_t \rangle^{n_s}} \exp\left(-\frac{p_T}{\langle p_t \rangle}\right). \quad (2)$$

In Eq. (2), the  $p_T$  of a given particle consists of  $p_{t1}$ ,  $p_{t2}$ , ...,  $p_{tn_s}$  of  $n_s$  partons. Here  $n_s$  is not large and it is around 2–5. This is because  $n_s$  is not determined by the collision system, but by the number of partons contributing to a given  $p_T$ . As for  $N$ , it is the number of particles, and it depends on the collision system. It is natural that  $\int_0^\infty f_1(p_T) dp_T = 1$  because  $f_1(p_T)$  is a probability density function.

### ii) *The Tsallis-Levy function*

The Tsallis-Levy function is one of the applications of the Tsallis statistics [31] in high-energy collisions. We have  $p_T$  distribution in form of the Tsallis-Levy function [30] to be

$$f_2(p_T) = \frac{1}{N} \frac{dN}{dp_T} = Cp_T \left(1 + \frac{\sqrt{p_T^2 + m_0^2} - m_0}{nT}\right)^{-(n+1)}. \quad (3)$$

Here  $T$  and  $n$  are free parameters,  $\sqrt{p_T^2 + m_0^2} = m_T$  is the transverse mass,  $m_0$  is the rest mass of the considered particle, and  $C$  is the normalization constant which is related to  $T$ ,  $n$ , and  $m_0$  to make  $\int_0^\infty f_2(p_T) dp_T = 1$ . Due to particle mass  $m_0$  appearing in  $\sqrt{p_T^2 + m_0^2} - m_0$  in Eq. (3),  $f_2(p_T)$  is related to  $m_0$ . Our tentative calculation shows that  $m_0$  affects mainly the normalization and weakly the tendency of the function.

In the fitting process of the  $p_T$  spectra with the Tsallis-Levy function [30], we can obtain  $T$  which is used to describe the excitation degree of system at the kinetic freeze-out stage. The influence of flow effect is included in  $T$

compared with  $T_0$ . In general,  $T > T_0$ , but in the  $\gamma p$  collision discussed in this work, due to the flow effect being small and considered negligible, we are of the opinion that  $T \approx T_0$  roughly. To obtain the excitation function of  $T$  more conveniently, we set  $n$  as a fixed value in the fitting with the Tsallis-Levy function [30].

iii) *Average transverse momentum and initial-state temperature*

In the process of fitting  $p_T$  spectra with the Erlang distribution [26–28],  $\langle p_T \rangle$  and  $T_i$  are estimated and used to describe the excitation degree of the system. In fact,  $\langle p_T \rangle$  can be obtained by

$$\langle p_T \rangle = \int_0^\infty p_T f_1(p_T) dp_T = n_s \langle p_t \rangle. \quad (4)$$

To obtain  $T_i$ , we need to use a color string percolation method [40–42] which gives

$$T_i = \sqrt{\frac{\langle p_T^2 \rangle}{2F(\xi)}}, \quad (5)$$

where

$$\langle p_T^2 \rangle = \int_0^\infty p_T^2 f_1(p_T) dp_T = n_s(n_s + 1) \langle p_t \rangle^2 \quad (6)$$

and  $F(\xi)$  is the color suppression factor. Although  $f_2(p_T)$  can be also used in the calculation of  $\langle p_T \rangle$  and  $\langle p_T^2 \rangle$ , it is more convenient to use  $f_1(p_T)$  from which specific results for  $\langle p_T \rangle$  and  $\langle p_T^2 \rangle$  can be obtained from the integration.

It is necessary to discuss the application of color string percolation method. In the process of using this method, we can determine the number of strings used. For instance, only one string is used in present work, that is to say  $F(\xi) = 1$  [43]. If we consider other strings, there will be the minimum  $F(\xi) \approx 0.6$  which results in the maximum increase of 29.1% in  $T_i$  [43]. Although it is possible to have any other strings in this work, they do not have a great influence on  $T_i$ . This is because one string accounts for a large proportion, but two and multiple strings account for a small one.

iv) *The squared momentum transfer*

In the center-of-mass reference frame, in two-body reaction  $2 + 1 \rightarrow 4 + 3$  or two-body-like reaction, three Mandelstam variables [33],  $s$ ,  $t$ , and  $u$  are defined. They are composed of four-momentum of participated particles and their forms are

$$s = -(P_1 + P_2)^2 = -(P_3 + P_4)^2, \quad (7)$$

$$t = -(P_1 - P_3)^2 = -(-P_2 + P_4)^2, \quad (8)$$

and

$$u = -(P_1 - P_4)^2 = -(-P_2 + P_3)^2, \quad (9)$$

respectively. Here,  $P_1$ ,  $P_2$ ,  $P_3$ , and  $P_4$  are four-momenta of particles 1, 2, 3, and 4, separately. Particle 1 is the target proton which is supposed to be incident along the  $Oz$  direction, and particle 2 is the incident  $\gamma$  which is supposed to be incident along the opposite direction. After collisions, particle 3 is the emitted proton which is emitted with angle  $\theta$  relative to the  $Oz$  direction, and particle 4 is the emitted meson which is emitted along the opposite direction.

Due to different forms of Mandelstam variables, the physical meanings of  $s$ ,  $t$ , and  $u$  are different.  $\sqrt{s}$  is supposed to be the center-of-mass energy, both  $-u$  and  $-t$  refer to the squared momentum transfer between particles. In this work, we choose variable  $-t$  to research, and its form is

$$|t| = |(E_1 - E_3)^2 - (\vec{p}_1 - \vec{p}_3)^2| = \left| m_1^2 + m_3^2 - 2E_1 \sqrt{\left( \frac{p_{3T}}{\sin \theta} \right)^2 + m_3^2} + 2\sqrt{E_1^2 - m_1^2} \frac{p_{3T}}{\tan \theta} \right|, \quad (10)$$

where  $E_1$  and  $E_3$ ,  $\vec{p}_1$  and  $\vec{p}_3$ , as well as  $m_1$  and  $m_3$  are the energy, momentum, and rest mass of particles 1 and 3 respectively. Besides,  $p_{3T}$  is the transverse momentum of particle 3 which obeys Eq. (2) or (3).

In this paper, we select the squared momentum transfer spectra at different center-of-mass energy  $W$  and incident photon energy  $E_\gamma$  to analyze. The center-of-mass energy is  $W = \sqrt{s} = \sqrt{-(P_1 + P_2)^2}$  in our analysis [24, 25]. Let  $Q^2$  and  $x_B$  be the squared photon virtuality and Bjorken scaling variable, and we have  $W^2 \simeq Q^2/x_B$  [44–51].

v) *The process of Monte Carlo calculations*

Although we can use Eq. (10) to obtain the single squared momentum transfer, its distribution is difficult to obtain. To obtain the squared momentum transfer distribution, we can execute the following steps. At first, we produce many concrete  $p_{3T}$  satisfied with Eq. (2) or (3) and  $\theta$ . At second, we can obtain many concrete squared momentum transfer by calculating with Eq. (10) repeatedly. At last, the squared momentum transfer distribution is obtained with the statistical method.

To produce many concrete  $p_{3T}$  and  $\theta$ , we may use the Monte Carlo method. Let  $R_{1,2}$  and  $r_{1,2,3,\dots,n_s}$  be random numbers distributed evenly in  $[0, 1]$ . Then, we obtain many concrete  $p_{3T}$  by solving this equation

$$\int_0^{p_T} f(p'_T) dp'_T < R_1 < \int_0^{p_T + \delta p_T} f(p'_T) dp'_T, \quad (11)$$

where  $\delta p_T$  is a small shift relative to  $p_T$ , and  $f(p'_T)$  represents Eq. (2) or (3). As for Eq. (2), there is a simpler expression of  $p_T$ . We can solve the equation

$$\int_0^{p_{tj}} f(p'_{tj}) dp'_{tj} = r_j \quad (j = 1, 2, 3, \dots, n_s), \quad (12)$$

which results in

$$p_{tj} = -\langle p_t \rangle \ln r_j \quad (j = 1, 2, 3, \dots, n_s). \quad (13)$$

In this way, the simpler expression is written as

$$p_T = \sum_{j=1}^{n_s} p_{tj} = -\langle p_t \rangle \sum_{j=1}^{n_s} \ln r_j = -\langle p_t \rangle \ln \left( \prod_{j=1}^{n_s} r_j \right). \quad (14)$$

The distribution of  $\theta$  satisfies with

$$f_\theta(\theta) = \frac{1}{2} \sin \theta \quad (15)$$

which is the half-sine function. In the source's rest frame, it is obtained under the assumption of isotropic emission. Solving the equation

$$\int_0^\theta f_\theta(\theta') d\theta' = R_2, \quad (16)$$

we have

$$\theta = 2 \arcsin \left( \sqrt{R_2} \right) \quad (17)$$

which is used in our calculations.

The squared momentum transfer distribution obtained using the above steps is used to fit the experimental data measured at different  $W$  and  $E_\gamma$ . In the fitting process, parameters  $\langle p_t \rangle$ ,  $n_s$ ,  $T$  are extracted with the method of least squares, and  $n$  is fixed to be large enough for convenience. Then, we can obtain  $\langle p_T \rangle$  from Eq. (4) and  $T_i$  from Eq. (5). The errors of parameters are obtained by the general method of statistical simulation.

### III. RESULTS AND DISCUSSION

Figure 1 shows the differential cross-section,  $d\sigma/d|t|$ , in the squared momentum transfer  $|t|$  of  $\gamma p \rightarrow \eta p$  produced in different center-of-mass energy ranges  $2.52 < W < 2.56$ ,  $2.60 < W < 2.64$ ,  $2.64 < W < 2.68$ ,  $2.68 < W < 2.72$ ,  $2.72 < W < 2.76$ ,  $2.76 < W < 2.80$ ,  $2.80 < W < 2.84$ ,  $2.84 < W < 2.88$ ,  $2.88 < W < 2.92$ ,  $2.92 < W < 2.96$ ,  $2.96 < W < 3.00$ ,  $3.04 < W < 3.08$ , and  $3.08 < W < 3.12$  GeV, corresponding to the incident photon energy range  $E_\gamma \in [2.91, 4.72]$  GeV. The black squares represent the experimental data performed at the CEBAF and measured by the CEBAF Large Acceptance Spectrometer (CLAS) Collaboration [34], where the data in  $2.56 < W < 2.60$  and  $3.00 < W < 3.04$  GeV are not available from the experiment. The green solid curves and red dash-dotted curves are the statistical results of  $|t|$  in which  $p_T$  satisfies the Erlang distribution and Tsallis-Levy function, respectively. One can see that the fitting results are in agreement with the experimental data.

Table 1. Values of  $\langle p_t \rangle$ ,  $n_s$ ,  $T_i$ ,  $T$ , and the first and last  $\chi^2/\text{ndof}$  corresponding to the statistical results of  $|t|$  in which  $p_T$  satisfies the Erlang distribution and Tsallis-Levy function, respectively, where  $E_\gamma$  is used for Figure 2(c) and  $W$  is used for other cases in Figures 1 and 2.

Figure	$W, E_\gamma$ (GeV)	$\langle p_t \rangle$ (GeV/c)	$n_s$	$T_i$ (GeV)	$\chi^2/\text{ndof}$	$T$ (GeV)	$\chi^2/\text{ndof}$
Figure 1	(2.52, 2.56)	$0.231 \pm 0.010$	3	$0.566 \pm 0.024$	32.76/17	$0.204 \pm 0.015$	33.62/18
	(2.60, 2.64)	$0.233 \pm 0.013$	3	$0.571 \pm 0.032$	22.93/16	$0.208 \pm 0.015$	23.63/17
	(2.64, 2.68)	$0.212 \pm 0.014$	3	$0.519 \pm 0.035$	27.79/16	$0.189 \pm 0.014$	26.76/17
	(2.68, 2.72)	$0.185 \pm 0.009$	3	$0.453 \pm 0.022$	20.99/16	$0.154 \pm 0.011$	21.47/17
	(2.72, 2.76)	$0.192 \pm 0.008$	3	$0.470 \pm 0.019$	14.69/16	$0.174 \pm 0.012$	14.21/17
	(2.76, 2.80)	$0.197 \pm 0.011$	3	$0.483 \pm 0.026$	9.59/16	$0.178 \pm 0.009$	8.83/17
	(2.80, 2.84)	$0.193 \pm 0.010$	3	$0.473 \pm 0.024$	14.40/16	$0.156 \pm 0.015$	14.42/17
	(2.84, 2.88)	$0.180 \pm 0.010$	3	$0.441 \pm 0.025$	20.97/15	$0.145 \pm 0.014$	20.68/16
	(2.88, 2.92)	$0.178 \pm 0.008$	3	$0.436 \pm 0.020$	2.63/13	$0.143 \pm 0.009$	2.67/14
	(2.92, 2.96)	$0.169 \pm 0.009$	3	$0.414 \pm 0.022$	6.19/15	$0.126 \pm 0.010$	5.54/16
	(2.96, 3.00)	$0.139 \pm 0.007$	3	$0.340 \pm 0.017$	8.64/11	$0.104 \pm 0.010$	8.52/12
	(3.04, 3.08)	$0.138 \pm 0.010$	3	$0.338 \pm 0.024$	7.28/11	$0.097 \pm 0.013$	7.14/12
(3.08, 3.12)	$0.133 \pm 0.006$	3	$0.326 \pm 0.015$	1.78/3	$0.092 \pm 0.010$	1.75/4	
Figure 2(a)	2.360	$0.172 \pm 0.003$	4	$0.544 \pm 0.010$	0.96/3	$0.199 \pm 0.006$	1.78/4
	2.551	$0.165 \pm 0.002$	4	$0.522 \pm 0.007$	0.70/3	$0.188 \pm 0.002$	1.39/4
Figure 2(b)	(2.694, 3.084)	$0.165 \pm 0.008$	4	$0.522 \pm 0.026$	5.87/3	$0.300 \pm 0.040$	9.46/4
Figure 2(c)	6	$0.118 \pm 0.005$	4	$0.373 \pm 0.016$	1.47/2	$0.097 \pm 0.007$	1.47/3
Figure 2(d)	2.895	$0.137 \pm 0.005$	4	$0.433 \pm 0.016$	9.78/9	$0.190 \pm 0.020$	21.75/10
	3.484	$0.129 \pm 0.006$	4	$0.408 \pm 0.019$	8.42/9	$0.182 \pm 0.013$	6.37/10
Figure 2(e)	2.895	$0.175 \pm 0.007$	4	$0.553 \pm 0.022$	12.21/2	$0.220 \pm 0.025$	13.92/3
	3.986	$0.152 \pm 0.005$	4	$0.481 \pm 0.015$	2.61/2	$0.158 \pm 0.013$	2.99/3

In the fitting process, the average transverse momentum  $\langle p_t \rangle$  contributed by participant partons, the number  $n_s$  of participant partons, and the effective temperature  $T$  of the emission source are extracted. With the values of  $\langle p_t \rangle$  and  $n_s$ , the average transverse momentum  $\langle p_T \rangle$  of final-state particles and the initial-state temperature  $T_i$  of the emission source are obtained naturally. To obtain  $T_0$  more conveniently, we take  $n = 40$  ( $q = 1.025$ ) in the Tsallis-Levy function [30]. Here,  $T_0 \approx T$  in the function for the small system  $\gamma p$  or  $ep$  process in which the effect of collective flow is neglected. In addition,  $E_1 = 0.938$  GeV in Eq. (10). In Table 1, we list the values of free parameters  $\langle p_t \rangle$  and  $n_s$ , derived parameter  $T_i$ , and  $\chi^2/\text{ndof}$  for the fit of Erlang distribution, as well as the values of free parameter  $T$  and  $\chi^2/\text{ndof}$  for the fit of Tsallis-Levy function.

Similar to Figure 1, Figure 2 presents the differential cross-section,  $d\sigma/d|t|$ , in  $|t|$  of (a, d, e)  $\gamma p \rightarrow \eta p$  and (b, c)

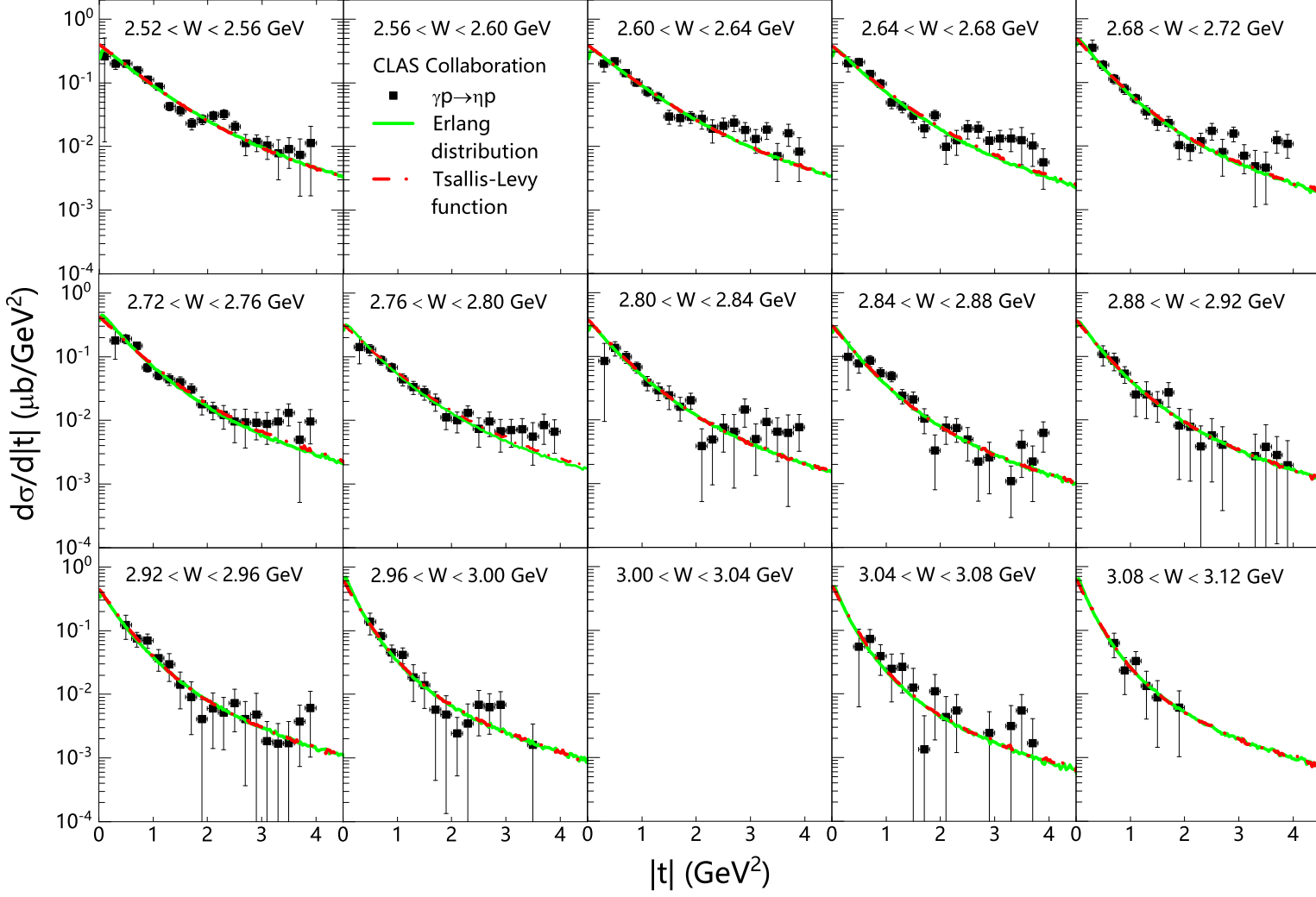


Figure 1. The differential cross-section  $d\sigma/d|t|$  in  $|t|$  of  $\gamma p \rightarrow \eta p$  process produced in  $ep$  collisions at energy ranges shown in the panels. The symbols represent the experimental data measured by the CLAS Collaboration [34], where the data in  $2.56 < W < 2.60$  and  $3.00 < W < 3.04$  GeV are not available from the experiment. The green solid curves and red dash-dotted curves are the statistical results of  $|t|$  in which  $p_T$  satisfies the Erlang distribution and Tsallis-Levy function, respectively.

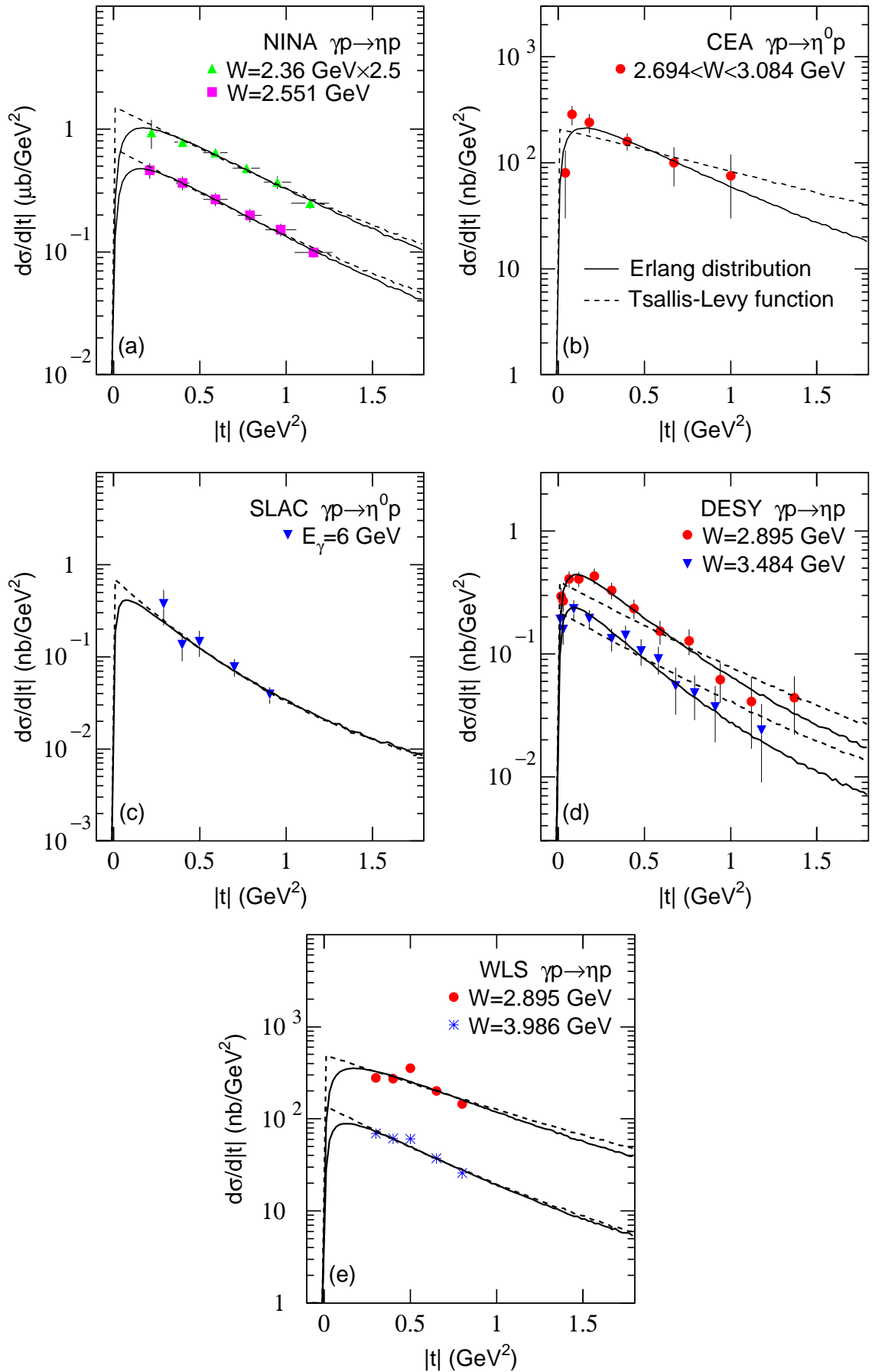


Figure 2. The differential cross-section  $d\sigma/d|t|$  in  $|t|$  of (a, d, e)  $\gamma p \rightarrow \eta p$  and (b, c)  $\gamma p \rightarrow \eta^0 p$  process produced at (a) NINA [35], (b) CEA [36], (c) SLAC [37], (d) DESY [38], and (e) WLS [39] at different  $W$  and  $E_\gamma$  shown in the panels. The symbols represent the experimental data [35–39]. The black solid curves and black dashed curves are the statistical results of  $|t|$  in which  $p_T$  satisfies the Erlang distribution and Tsallis-Levy function, respectively.



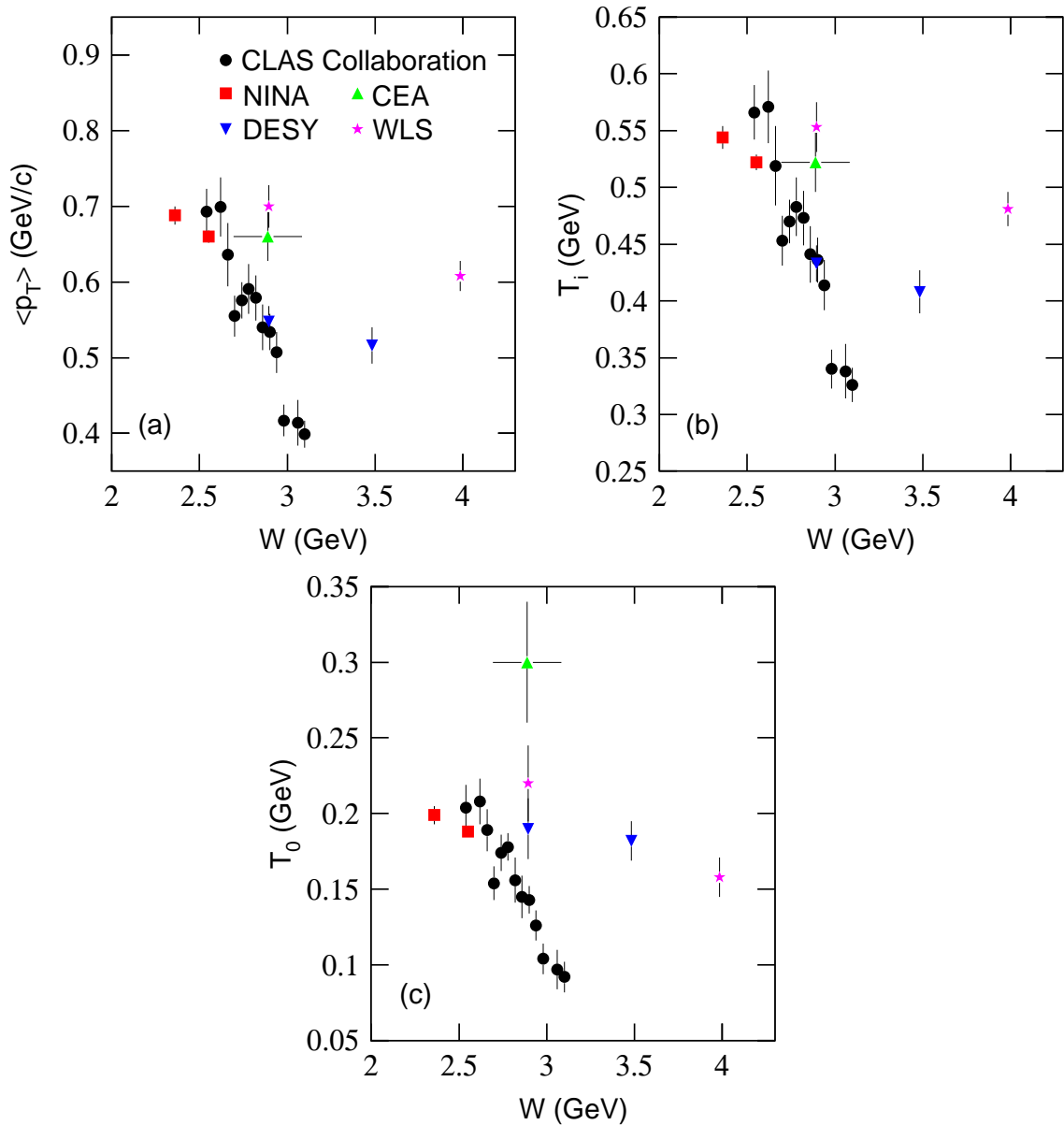


Figure 3. The dependences of (a)  $\langle p_T \rangle$ , (b)  $T_i$ , and (c)  $T_0$  on  $W$  in  $ep$  collisions produced at different devices.

$\gamma p \rightarrow \eta^0 p$  produced at (a) NINA [35], (b) CEA [36], (c) SLAC [37], (d) DESY [38], and (e) WLS [39] at (a)  $W = 2.36, 2.551$  GeV, in (b)  $2.694 \text{ GeV} < W < 3.084$  GeV, at (c)  $E_\gamma = 6$  GeV, (d)  $W = 2.895, 3.484$  GeV, and (e)  $W = 2.895, 3.986$  GeV. The symbols in Figure 2 represent the experimental data. The black solid and dashed curves are the statistical results of  $|t|$  in which  $p_T$  satisfies the Erlang distribution and Tsallis-Levy function, respectively. The values of parameters and  $\chi^2/\text{ndof}$  are listed in Table 1. One can see that the statistical results are in approximate agreement with the experimental data.

The dependences of (a)  $\langle p_T \rangle$ , (b)  $T_i$ , and (c)  $T_0$  on center-of-mass energy ( $W$ ) are given in Figure 3. The different symbols represent the parameter values extracted from Figures 1 and 2. For the results from the CLAS Collaboration, one can see that  $\langle p_T \rangle$ ,  $T_i$ , and  $T_0$  decrease generally with an increase in  $W$ . For the results from the other cases, the trends are not clear. In the fitting process of experimental data produced at CEA and DESY, we consider that the ranges of  $|t|$  are wider than others. To fit better, there is a big difference between the statistical results of  $|t|$  in which  $p_T$  satisfies the Erlang distribution and Tsallis-Levy function, and it results in a higher  $T_0$  extracted from the

statistical results of  $|t|$  in which  $p_T$  satisfies the Tsallis-Levy function.

From Figure 3, it should be noted that the results for CEA and WLS overlap for  $\langle p_T \rangle$  and  $T_i$ , but differ significantly for  $T_0$ , at  $W \approx 3$  GeV. The reason is that both  $\langle p_T \rangle$  and  $T_i$  are from the Erlang distribution and  $T_0$  is from the Tsallis-Levy function. In most cases, the two fits are similar to each other. In a few cases (Figures 2(b) and 2(d)), the two fits (the solid and dashed curves) are inharmonic. If we try to obtain a similar result for the two fits in a given range of  $|t|$  (e.g.  $|t| > 0.2$  GeV<sup>2</sup>), a few data (the first or second one) will deviate greatly from the fit. That is, we may adjust the parameters in Figure 3(c) to be harmonious. However, a worse fit will be obtained. Due to the two inharmonic fits in Figures 2(b), if the two fits of the Erlang distribution in Figures 2(b) and 2(e) are harmonious (Figures 3(a) and 3(b)), the two fits of the Tsallis-Levy function in the two panels are inharmonic (Figure 3(c)). In addition, because two parameters are used in the Erlang distribution and one parameter is used in Tsallis-Levy function, the former is more flexible than the latter in the fit.

Generally speaking,  $\langle p_T \rangle$ ,  $T_i$ , and  $T_0$  increase with the increase of  $W$  in heavy-ion collisions at a few GeV energy [10, 17–21, 23, 43] which is the energy range discussed in this work. Comparing with heavy-ion collisions, in  $\gamma p \rightarrow \eta p$  reaction the situation is different due to the absence of secondary collision process and cold nuclear effect in the small system. In addition, the small system has not enough time to react at higher energy. This implies that the small system has a lower excitation degree at higher energy. Although this work confirms our previous work [24], the energy range discussed by us is narrow, and the data cited here are measured at different devices with low statistics and large errors in most cases. To obtain more solid and explicit conclusions regarding the evolution of the parameters with changing the energy, significantly higher statistics of the experimental data are required in the future.

Before summary and conclusions, we would like to point out that although the multiplicity is only two in the two-body reaction discussed in the present work, we have used the parametrization from the Erlang distribution and Tsallis-Levy function due to lots of events being collected in experiments. This case can be compared with the grand canonical ensemble in statistical physics. Although the particles in different events do not have interactions and the multiplicity in each event is very low, these particles have the same or similar production condition due to the same or similar events with given collision energy. Therefore, we think that the particles in lots of events obey some statistical laws. In addition, as a reflection of the average kinetic energy of the thermal or disorganized motion, the concept of temperature is applicable in the field of high energy collisions, even two-body reaction.

#### IV. SUMMARY AND CONCLUSIONS

The squared momentum transfer spectra of  $\eta$  and  $\eta^0$  produced in the two-body process  $\gamma p \rightarrow \eta(\eta^0) + p$  have been analyzed by the statistical results of  $|t|$  in which  $p_T$  satisfies the Erlang distribution and Tsallis-Levy function respectively. The squared momentum transfer undergoes from the incident  $\gamma$  to emitted  $\eta$  or  $\eta^0$ , or also equivalently from the target proton to emitted proton. The statistical results are in agreement with the experimental data measured at different experiments. In the fitting process, free parameters  $\langle p_t \rangle$ ,  $n_s$ , and  $T$  are extracted. Then, we obtain the dependences of  $\langle p_T \rangle$ ,  $T_i$ , and  $T_0$  on center-of-mass energy  $W$ .

At a few GeV, it is believed that  $\langle p_T \rangle$ ,  $T_i$ , and  $T_0$  increase generally with an increase in  $W$  in heavy-ion collisions. However, in  $\gamma p \rightarrow \eta p$  reaction the situation is different due to the absence of secondary collision process and cold nuclear effect in the small system. Meanwhile, the small system has not enough time to react at higher energy. This implies that the small system has a lower excitation degree at higher energy. The excitation functions of the concerned parameters in the large and small systems have different tendencies. More data are required in the future to compare the excitation functions in the two kinds of systems.

**Author Contributions:** The authors contributed to the paper in this way: conceptualization, F.-H.L. and K.K.O.; methodology, F.-H.L. and K.K.O.; software, Q.W.; validation, F.-H.L. and K.K.O.; formal analysis, Q.W.;

investigation, Q.W.; resources, Q.W.; data curation, Q.W.; writing – original draft preparation, Q.W.; writing – review and editing, F.-H.L. and K.K.O.; visualization, Q.W.; supervision, F.-H.L. and K.K.O.; project administration, Q.W. and F.-H.L.; funding acquisition, Q.W., F.-H.L. and K.K.O. All authors have read and agreed to the published version of the manuscript.

**Funding:** The work of Q.W. was supported by the Shanxi Provincial Natural Science Foundation under Grant No. 2023 and the Doctoral Scientific Research Foundations of Shanxi Province and Shanxi Institute of Energy. The work of F.-H.L. was supported by the National Natural Science Foundation of China under Grant No. 12147215, the Shanxi Provincial Natural Science Foundation under Grant No. 202103021224036, and the Fund for Shanxi “1331 Project” Key Subjects Construction. The work of K.K.O. was supported by the Ministry of Innovative Development of the Republic of Uzbekistan within the fundamental project No. F3-20200929146 on analysis of open data on heavy-ion collisions at RHIC and LHC.

**Institutional Review Board Statement:** Not applicable.

**Informed Consent Statement:** Not applicable.

**Data Availability Statement:** The data used to support the findings of this study are included within the article and are cited at relevant places within the text as references.

**Conflicts of Interest:** The authors declare that there are no conflicts of interest regarding the publication of this paper. The funders had no role in the design of the study; in the collection, analysis, or interpretation of the data; in the writing of the manuscript; or in the decision to publish the results.

## References

- 
- [1] Caines, H. What’s interesting about strangeness production? An overview of recent results. *J. Phys. G* **2005**, *31*, S101–S117.
  - [2] Shuryak, E.V. Quantum chromodynamics and the theory of superdense matter. *Phys. Rep.* **1980**, *61*, 71–158.
  - [3] Digal, S.; Petreczky, P.; Satz, H. Quarkonium feed-down and sequential suppression. *Phys. Rev. D* **2001**, *64*, 094015.
  - [4] Karsch, F.; Kharzeev, D.; Satz, H. Sequential charmonium dissociation. *Phys. Lett. B* **2006**, *637*, 75–80.
  - [5] Braun-Munzinger, P.; Stachel, J. The quest for the quark-gluon plasma. *Nature* **2007**, *448*, 302–309.
  - [6] Wang, H.; Chen, J.-H.; Ma, Y.-G.; Zhang, S. Charm hadron azimuthal angular correlations in Au+Au collisions at  $\sqrt{s_{NN}} = 200$  GeV from parton scatterings. *Nucl. Sci. Tech.* **2019**, *30*, 185.
  - [7] Yan, T.-Z.; Li, S.; Wang, Y.-N.; Xie, F.; Yan, T.-F. Yield ratios and directed flows of light particles from proton-rich nuclei-induced collisions. *Nucl. Sci. Tech.* **2019**, *30*, 15.
  - [8] Fisli, M.; Mebarki, N. Top quark pair-production in noncommutative standard model. *Adv. High Energy Phys.* **2020**, *2020*, 7279627.
  - [9] He, X.-W.; Wu, F.-M.; Wei, H.-R.; Hong, B.-H. Energy-dependent chemical potentials of light hadrons and quarks based on transverse momentum spectra and yield ratios of negative to positive particles. *Adv. High Energy Phys.* **2020**, *2020*, 1265090.
  - [10] Waqas, M.; Li, B.-C. Kinetic freeze-out temperature and transverse flow velocity in Au-Au collisions at RHIC-BES energies. *Adv. High Energy Phys.* **2020**, *2020*, 1787183.
  - [11] Tang, Z.-B.; Zha, W.-M.; Zhang, Y.-F. An experimental review of open heavy flavor and quarkonium production at RHIC.

*Nucl. Sci. Tech.* **2020**, *31*, 81.

- [12] Shen, C.; Yan, L. Recent development of hydrodynamic modeling in heavy-ion collisions. *Nucl. Sci. Tech.* **2020**, *31*, 122.
- [13] Yu, H.; Fang, D.-Q.; Ma, Y.-G. Investigation of the symmetry energy of nuclear matter using isospin-dependent quantum molecular dynamics. *Nucl. Sci. Tech.* **2020**, *31*, 61.
- [14] Bhaduri, S.; Bhaduri, A.; Ghosh, D. Study of di-muon production process in  $pp$  collision in CMS data from symmetry scaling perspective. *Adv. High Energy Phys.* **2020**, *2020*, 4510897.
- [15] Tawfik, A.N. Out-of-equilibrium transverse momentum spectra of pions at LHC energies. *Adv. High Energy Phys.* **2019**, *2019*, 4604608.
- [16] Nayak, J.K.; Alam, J.; Sarkar, S.; Sinha, B. Measuring initial temperature through a photon to dilepton ratio in heavy-ion collisions. *J. Phys. G* **2008**, *35*, 104161.
- [17] Adare, A. et al. [PHENIX Collaboration]. Enhanced production of direct photons in Au+Au collisions at  $\sqrt{s_{NN}} = 200$  GeV and implications for the initial temperature. *Phys. Rev. Lett.* **2010**, *104*, 132301.
- [18] Csanád, M.; Májér, I. Initial temperature and EoS of quark matter via direct photons. *Phys. Part. Nuclei Lett.* **2011**, *8*, 1013–1015.
- [19] Csanád, M.; Májér, I. Equation of state and initial temperature of quark gluon plasma at RHIC. *Cent. Eur. J. Phys.* **2012**, *10*, 850–857.
- [20] Soltz, R.A.; Garishvili, I.; Cheng, M.; Abelev, B.; Glenn, A.; Newby, J.; Levy, L.A.L.; Pratt, S. Constraining the initial temperature and shear viscosity in a hybrid hydrodynamic model of  $\sqrt{s_{NN}} = 200$  GeV Au+Au collisions using pion spectra, elliptic flow, and femtoscopic radii. *Phys. Rev. C* **2013**, *87*, 044901.
- [21] Waqas, M.; Liu, F.-H. Initial, effective, and kinetic freeze-out temperatures from transverse momentum spectra in high-energy proton(deuteron)-nucleus and nucleus-nucleus collisions. *Eur. Phys. J. Plus* **2020**, *135*, 147.
- [22] Cleymans, J.; Paradza, M.W. Tsallis statistics in high energy physics: chemical and thermal freeze-outs. *Physics* **2020**, *2*, 654–664.
- [23] Li, L.-L.; Liu, F.-H. Kinetic freeze-out properties from transverse momentum spectra of pions in high energy proton-proton collisions. *Physics* **2020**, *2*, 277–308.
- [24] Wang, Q.; Liu, F.-H.; Olimov, K.K. Initial- and final-state temperatures of emission source from differential cross-section in squared momentum transfer in high-energy collisions. *Adv. High Energy Phys.* **2021**, *2021*, 6677885.
- [25] Wang, Q.; Liu, F.-H.; Olimov, K.K. Initial-state temperature of light meson emission source From squared momentum transfer spectra in high-energy collisions. *Front. Phys.* **2021**, *9*, 792039.
- [26] Liu, F.-H.; Li, J.-S. Isotopic production cross section of fragments in  $^{56}\text{Fe}+p$  and  $^{136}\text{Xe} (^{124}\text{Xe})+\text{Pb}$  reactions over an energy range from 300A to 1500A MeV. *Phys. Rev. C* **2008**, *78*, 044602.
- [27] Liu, F.-H. Unified description of multiplicity distributions of final-state particles produced in collisions at high energies. *Nucl. Phys. A* **2008**, *810*, 159–172.
- [28] Liu, F.-H.; Gao, Y.-Q.; Tian, T.; Li, B.-C. Unified description of transverse momentum spectrums contributed by soft and hard processes in high-energy nuclear collisions. *Eur. Phys. J. A* **2014**, *50*, 94.
- [29] Hagedorn, R. Multiplicities,  $p_T$  distributions and the expected hadron  $\rightarrow$  quark-gluon phase transition. *Riv. Nuovo Cim.* **1983**, *6(10)*, 1–50.
- [30] Abelev, B. et al. [ALICE Collaboration]. Production of  $\Sigma(1385)^\pm$  and  $\Xi(1530)^0$  in proton-proton collisions at  $\sqrt{s} = 7$  TeV. *Eur. Phys. J. C* **2015**, *75*, 1–19.
- [31] Tsallis, C. Possible generalization of Boltzmann-Gibbs statistics. *J. Stat. Phys.* **1988**, *52*, 479–487.
- [32] Abelev, B.I. et al. [STAR Collaboration]. Strange particle production in  $p + p$  collisions at  $\sqrt{s} = 200$  GeV. *Phys. Rev. C* **2007**, *75*, 064901.
- [33] Zhang, N.-S. *Particle Physics (Volume I)*; Science Press; Beijing, China, **1986**.
- [34] Hu, T. et al. [CLAS Collaboration]. Photoproduction of  $\eta$  mesons off the proton for  $1.2 < E_\gamma < 4.7$  GeV using CLAS at Jefferson Laboratory. *Phys. Rev. C* **2020**, *102*, 065203.
- [35] Bussey, P.J.; Raine, C.; Rutherglen, J.G.; Booth, P.S.L.; Carroll, L.J.; Daniel, P.R.; Edwards, A.W.; Hardwick, C.J.; Holt, J.R.; Jackson, J.N. et al. The polarized beam asymmetry in photoproduction of eta mesons from protons at 2.5 GeV and

- 3.0 GeV. *Phys. Lett. B* **1976**, *61*, 479–482.
- [36] Bellenger, D.; Deutsch, S.; Luckey, D.; Osborne, L.S.; Schwitters, R. Photoproduction of  $\eta^0$  mesons at 4 GeV. *Phys. Rev. Lett.* **1968**, *21*, 1205–1208.
- [37] Anderson, R.; Gustavson, D.; Johnson, J.; Ritson, D.; Jones, W.G.; Kreinick, D.; Murphy, F.; Weinstein, R. Measurements of  $\pi^0$  and  $\eta^0$  photoproduction at incident gamma-ray energies of 6.0–17.8 GeV. *Phys. Rev. Lett.* **1968**, *21*, 384–386.
- [38] Braunschweig, W.; Erlewein, W.; Frese, H.; Lübelsmeyer, K.; Meyer-Wachsmuth, H.; Schmitz, D.; Schultz von Dratzig, A.; Wessels, G. Single photoproduction of  $\eta$ -mesons of hydrogen in the forward direction at 4 and 6 GeV. *Phys. Lett. B* **1970**, *33*, 236–240.
- [39] Dewire, J.; Gittelmann, B.; Loe, R.; Loh, E.C.; Ritchie, D.J.; Lewis, R.A. Photoproduction of eta mesons from hydrogen. *Phys. Lett. B* **1971**, *37*, 326–328.
- [40] Gutay, L.J.; Hirsch, A.S.; Scharenberg, R.P.; Srivastava, B.K.; Pajares, C. De-confinement in small systems: clustering of color sources in high multiplicity  $\bar{p}p$  collisions at  $\sqrt{s} = 1.8$  TeV. *Int. J. Mod. Phys. E* **2015**, *24*, 1550101.
- [41] Scharenberg, R.P.; Srivastava, B.K.; Pajares, C. Exploring the initial stage of high multiplicity proton-proton collisions by determining the initial temperature of the quark-gluon plasma. *Phys. Rev. D* **2019**, *100*, 114040.
- [42] Sahoo, P.; De, S.; Tiwari, S.K.; Sahoo, R. Energy and centrality dependent study of deconfinement phase transition in a color string percolation approach at RHIC energies. *Eur. Phys. J. A* **2018**, *54*, 136.
- [43] Wang, Q.; Liu, F.-H. Excitation function of initial temperature of heavy flavor quarkonium emission source in high energy collisions. *Adv. High Energy Phys.* **2020**, *2020*, 5031494.
- [44] Aaron, F.D. et al. [H1 Collaboration]. Diffractive electroproduction of  $\rho$  and  $\phi$  mesons at HERA. *J. High Energy Phys.* **2010**, *2010(05)*, 032.
- [45] Aktas, A. et al. [H1 Collaboration]. Elastic  $J/\psi$  production at HERA. *Eur. Phys. J. C* **2006**, *46*, 585–603.
- [46] Chekanov, S. et al. [ZEUS Collaboration]. Exclusive  $\rho^0$  production in deep inelastic scattering at HERA. *PMC Phys. A* **2007**, *1*, 6.
- [47] Derrick, M. et al. [ZEUS Collaboration]. Measurement of elastic  $\omega$  photoproduction at HERA ZEUS Collaboration. *Z. Phys. C* **1997**, *73*, 73–84.
- [48] Chekanov, S. et al. [ZEUS Collaboration]. Exclusive electroproduction of  $\phi$  mesons at HERA. *Nucl. Phys. B* **2005**, *718*, 3–31.
- [49] Chekanov, S. et al. [ZEUS Collaboration]. Exclusive electroproduction of  $J/\psi$  mesons at HERA. *Nucl. Phys. B* **2004**, *695*, 3–37.
- [50] Barberis, D. et al. [WA102 Collaboration]. A coupled channel analysis of the centrally produced  $K^+K^-$  and  $\pi^+\pi^-$  final states in  $pp$  interactions at 450 GeV/c. *Phys. Lett. B* **1999**, *462*, 462–470.
- [51] Barberis, D. et al. [WA102 Collaboration]. A measurement of the branching fractions of the  $f_1(1285)$  and  $f_1(1420)$  produced in central  $pp$  interactions at 450 GeV/c. *Phys. Lett. B* **1998**, *440*, 225–232.